www.MaterialsViews.com

Facile Synthesis of pH-sensitive Germanium Nanocrystals with High Quantum Yield for Intracellular Acidic Compartment Imaging

Feng Li, Jing Wang, Shuqing Sun, Hai Wang, Zhiyong Tang, and Guangjun Nie**

***A** green-light emitting germanium nanocrystal-based biosensor to monitor lysosomal pH changes is developed. The Ge nanocrystals are synthesized in an aqueous solution with a significantly enhanced photoluminescence quantum yield of 26%. This synthesis involves a facile solution based route which avoided the use of toxic or environmentally unfriendly agents. Importantly, the photoluminescence intensity of the synthesized Ge nanocrystals is particularly sensitive to changes in pH between 5 and 6. When incubated with cultured cells, the nanocrystals are internalized and subsequently translocated via the lysosomal pathway, and the Ge nanocrystals' fluorescence are greatly enhanced, even when the lysosomal pH is only slightly increased. These results reveal that the Ge nanocrystals possess high pH sensitivity compared to a commercially available dye, LysoSensor Green DND-189. The fluorescent properties of the Ge nanocrystals are demonstrated to be dependent on both the crystal form and their surface chemistry. The superior fluorescence properties and bioapplicability of the Ge nanocrystals makes them a promising intracellular bioimaging probe for monitoring various pH-sensitive processes in cells.*

F. Li, J. Wang, H. Wang, Prof. G. Nie
CAS Key Laboratory for Biomedical Effects
of Nanomaterials & Nanosafety
National Center for Nanoscience and Technology
Beijing 100190, China
E-mail: niegj@nanoctr.cn
F. Li, Prof. S. Sun
Institute of Optical Imaging and Sensing, Shenzhen
Key Laboratory for Minimal Invasive Medical Technologies
Graduate School at Shenzhen
Tsinghua University
Shenzhen 518055, China
E-mail: sun.shuqing@sz.tsinghua.edu.cn
Z. Tang
Laboratory of Nanomaterials
National Center for Nanoscience and Technology
Beijing 100190, China
Prof. S. Sun
Department of Physics,
Tsinghua University
Beijing 100084, China
DOI: 10.1002/smll.201402743

1. Introduction

Colloidal photoluminescent nanocrystals have long been regarded as attractive optical probes due to their unique optical properties, including their narrow emission band, broad absorption band, tunable emission peak, long fluorescent lifetime, and high photobleaching resistance. Since the first successful demonstrations of photoluminescent nanocrystals used to label cells by the Alivisators and Nie Groups,[1] they have been widely applied as luminescent cell probes.[2] However, the applicability of heavy metal-based photoluminescent nanocrystals in biosensing and bioimaging has been hindered by their potential toxicity. Because of the intrinsic toxic nature of the semiconductor materials themselves and the necessity of a phase transfer procedure after the photoluminescent nanocrystals are first obtained in organic solvents, most photoluminescent nanocrystals require sophisticated optimization for biological applications to avoid potential cytotoxicity.[3] In recent years, the development of heavy element-free photoluminescent nanocrystals

has attracted considerable interest, being viewed as more practical and far-sighted than the traditional toxic core-coating strategies.[4]

Group IV semiconductor silicon (Si) and germanium (Ge) nanocrystals are promising materials for bio-applicable photoluminescent nanocrystals with low toxicity and high biocompatibility. While a considerable research has been implemented on Si nanocrystals,[5] relatively few studies have investigated Ge nanocrystals, despite Ge's much larger excitonic Bohr radius (11.5 nm) relative to Si (4 nm).[6] Current synthesis methods for fluorescent Ge nanocrystals (e.g., rf-magnetron cosputtering methods,[7] reductive thermal decompositions of solid-state polymers,[8] supercritical fluid assisted thermolyses of metal-organic complexes,[9] hydrogermylation-based methods,[10] metathesis reactions,[11] colloidal syntheses,[12] and solution-phase thermal decompositions[13] commonly involve toxic Ge precursors and environmentally unfriendly organic reagents. These nanocrystals also require complicated post-synthesis treatments of photoluminescent nanocrystals before they can be used in biological applications. In addition, these methods often use unstable and strong reducing agents and rely on high temperature or oxygen-free synthesis conditions. Recently, Hu et al. reported a solution based route for the synthesis of Ge nanocrystals in a communication,[6c] however the full details were not fully explored.

In this study, we developed the aqueous-solution based route for the synthesis of blue-emitting Ge nanocrystals with both cubic and β-Sn tetragonal structures under mild conditions. The photoluminescence quantum yield of these nanocrystals was determined to be as large as approximately 26%. Germanium dioxide (GeO_2) was used as the Ge precursor instead of the toxic organogermanium or germanium halide compounds reported previously. Due to their pH-dependent fluorescent properties, the synthesized Ge nanocrystals have been tested for their use as intracellular pH sensors for acidic organelles in live-cell imaging. Moreover, the photoluminescent Ge nanocrystals prepared in aqueous solution have no measurable cytotoxicity, making them particularly well-suited for potential biological applications.

2. Synthesis and Characterization

2.1. Synthesis of Ge Nanocrystals

The Ge nanocrystals were prepared as follows. Firstly, GeO_2 was dissolved in a NaOH solution under ultrasonication to create aqueous Na_2GeO_3. The pH of this solution was adjusted to 6.5 with HCl. Next, polyvinylpyrrolidone (PVP Mw = 58 000) was dissolved in a $NaBH_4$ solution while stirring followed by injection of the prepared Na_2GeO_3 solution. The reaction mixture was incubated in an oil bath at 80 °C for 8 h. The color of the reaction mixture exhibited a series of changes shown in **Figure 1**a. After adding Na_2GeO_3, the colorless aqueous solution turned to yellow-green, which

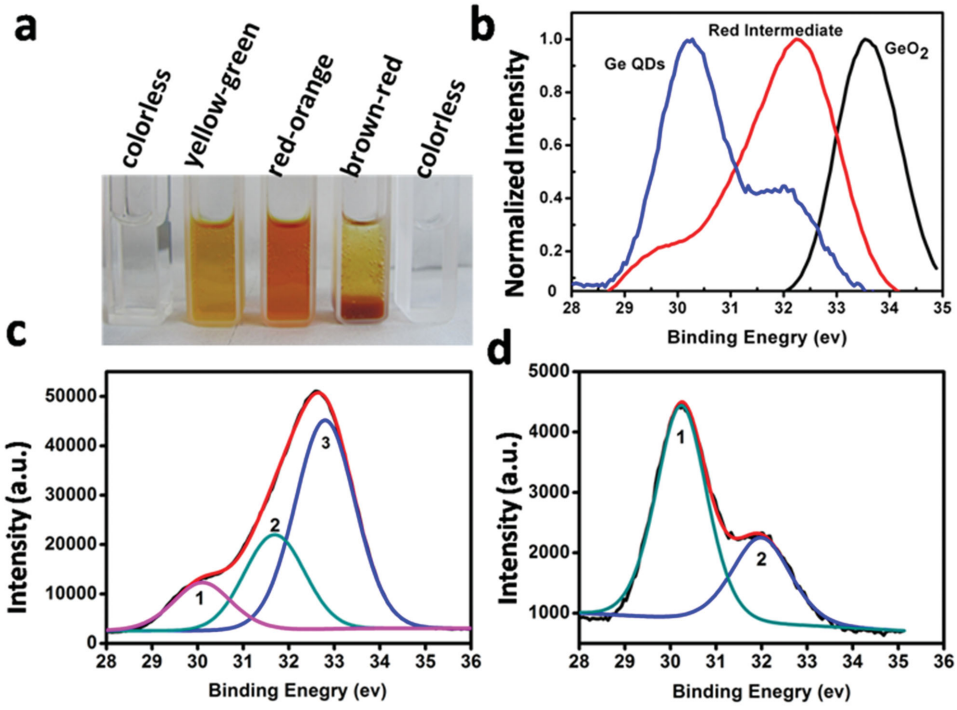

Figure 1. a) Color changes of the solution during the formation of the Ge nanocrystals; b) X-ray photoelectron spectra of the GeO_2 power, the intermediate precipitate, and the Ge nanocrystal product showing the oxidation state changes; c) Deconvolution of the X-ray photoelectron spectra of the intermediate precipitate with separated assigned peaks; d) Deconvolution of the X-ray photoelectron spectra of the Ge nanocrystals with separated assigned peaks. Suboxide species (labeled as 2 and 3) were determined to be the main components in (c), while germanium (labeled as 1) was the dominating component in (d).

changed to red-orange before forming a large amount of brown-red precipitate. Finally, the pH of the mixture was adjusted to 8 to 9 to dissolve the precipitate and to generate the colorless Ge nanocrystals. These Ge nanocrystals were separated from the resulting system by ultrafiltration. Figure 1b shows the Ge 3d photoemission spectra obtained from the GeO_2 powder, the intermediate precipitate and the Ge nanocrystals by X-ray surface photoelectron spectroscopy (XPS).[6a] Prolonged reduction resulted in complex mixtures of GeOx ($2 > x \geq 0$) in the precipitate, as shown in Figure 1b,c, with suboxide species (labeled as 2 and 3) being the main species. Notably, the Ge nanocrystals consist of mainly elemental germanium despite the presence of the remaining suboxide species (Figure 1b,d).

2.2. TEM and Fourier Transform Infrared Spectroscopy Characterization

Morphological, dimensional and crystallographic characteristics of the Ge nanocrystals were obtained by transmission electron microscopy (TEM) (**Figure 2**) and dynamic light scattering (DLS) (Figure S1 in supporting information). It is evident that the Ge nanocrystals have a rather narrow size distribution of approximately 3 to 7 nm, and high-resolution TEM (HRTEM) images of single Ge nanocrystals further demonstrate a typical lattice spacing of 2 Å (inset Figure 2b). This result is in accordance with the (220) d-spacing of cubic Ge. Interestingly, in addition to cubic Ge, unexpected crystal lattices belonging to the β-Sn tetragonal structure is also identified in the X-ray diffraction (XRD) pattern survey (Figure S2) and fast Fourier transform HRTEM (the results has been highlighted in Table S1). This observation disagrees with a previous report, which states that the β-Sn tetragonal structure of Ge only can be prepared under extreme conditions, such as high pressure.[14] XRD patterns of as-synthesized products had two broad peaks due to the small size effect or the surface protective agent effects. While the characteristic peaks belonged to β-Sn tetragonal and cubic Ge has been detected in XRD spectra after being annealed at 600 °C under Ar gas condition, Table S1 summarized some results from HRTEM and the main peaks shown in Figure S2, and the unidentified peaks might come from some impurities.[12a,15] Excluding the Ge cores, the surface state of the Ge nanocrystals was also explored by Fourier transform infrared spectroscopy (FTIR) measurement (Figure 2c). One can distinguish two characteristic peaks at 1650 cm^{-1} and 2900–3000 cm^{-1} due to the C=O and C–H stretching modes similar to those of PVP, indicating that the polymer is coating the surface of the Ge nanocrystals. The new peak in the Ge nanocrystals at 1078 cm^{-1} can be attributed to Ge–O–C species,[9] suggesting that the PVP layer is attached to the particle surface via chemisorption. We also notice that the peak corresponding to Ge–O–Ge stretches at 850 cm^{-1} derived from germanium oxide cannot be detected in the FTIR spectrum, which is in agreement with the XPS analysis that most of the germanium oxide has been reduced to pure Ge metal inside nanocrystals (Figure 1d). We hypothesized that $NaGeO_4$ was first reduced to yellow Ge^{2+} and hydrolyzed to form a yellow precipitate, followed by dehydration and result in brown precipitate of GeO. Finally the precipitation was gradually reduced to Ge with the protection of PVP.

2.3. UV–Visible Absorption and Photoluminescence Characterization

The optical properties of the Ge nanocrystals are observed in the UV–visible absorption spectrum at room temperature (**Figure 3**a). The absorption peaks at 334 nm and 268 nm correspond to photo energies of 3.71 eV and 4.63 eV (inset Figure 2a), which are associated with the direct band transitions at L and X, respectively. Significant blue shifts are observed in comparison to the corresponding peaks of bulk Ge at 550 nm (2.1 eV) and 280 nm (4.3 eV),[16] which are most likely due to quantum confinement effects.[9]

The photoluminescence spectra of the Ge nanocrystals at room temperature with different excitation wavelengths have also been measured, with the maximum emission achieved at approximately 446 nm under 365 nm excitation (Figure 3b). Excitation wavelengths lower than 350 nm produced a different emission peak at 395 nm (Figure S3), while two peaks (395 nm and 446 nm) were present in the photoluminescence spectrum under 350 nm excitation (Figure 3c). With excitation wavelengths of 365 nm and above, the 395 nm peak disappeared, and intensity of the 446 nm peak decreased as the excitation wavelength shifted toward red. We hypothesized that the two independent emission peaks at 395 and

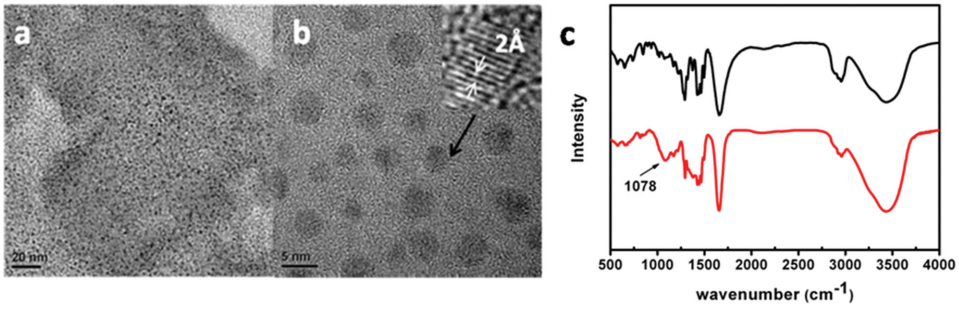

Figure 2. a,b) TEM images of the obtained Ge nanocrystals at different scales. Inset: HRTEM image of a single Ge nanocrystal, in which the lattice spacing, measured by fast Fourier transform, matches the (220) d-spacing of cubic Ge. c) FTIR spectra of PVP (black) and PVP-coated Ge nanocrystals (red).

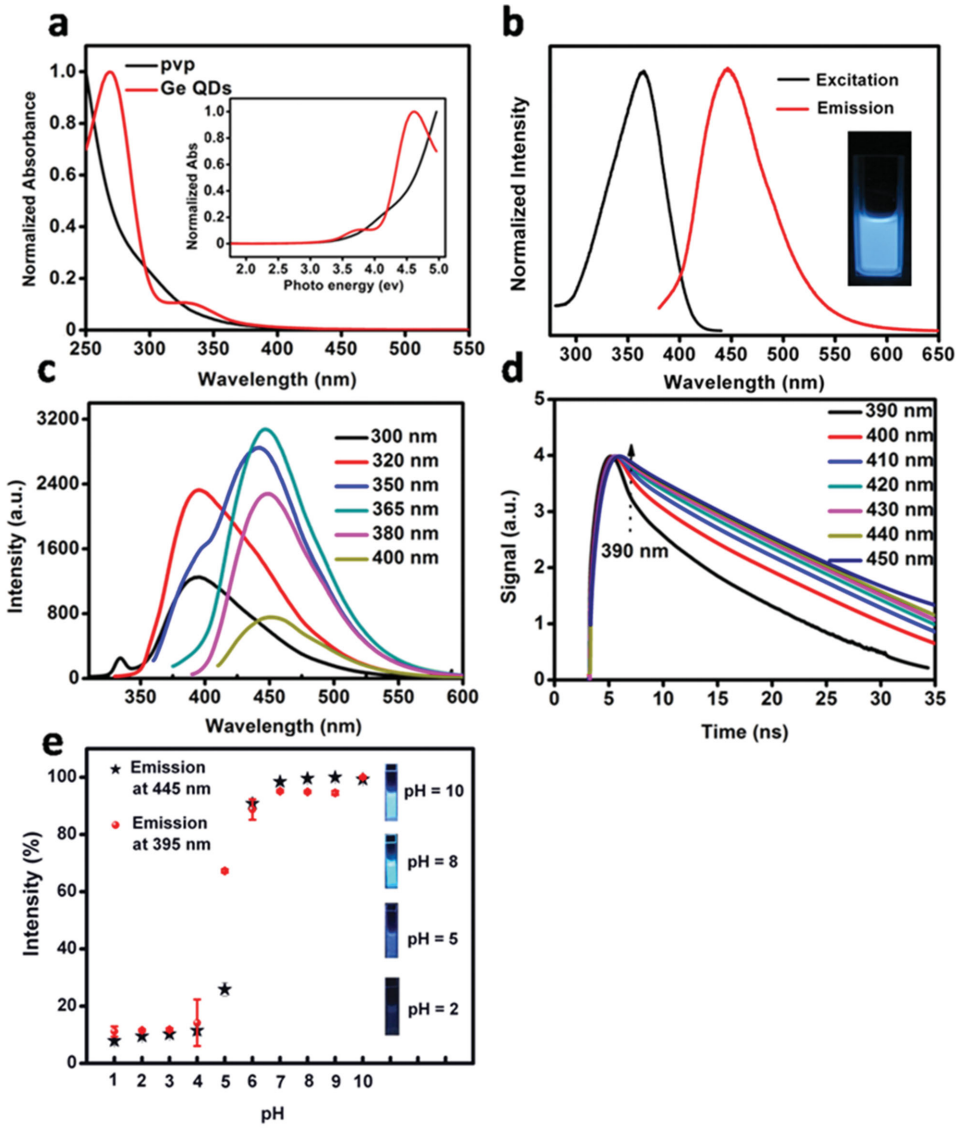

Figure 3. Characterization of UV–visible absorption and photoluminescence properties. a) UV–visible absorption spectra of the Ge nanocrystals (red) and solvent PVP (black) at room temperature. Inset: optical band gap of Ge nanocrystals estimated from the absorption spectrum. b) Photoluminescence spectrum of Ge nanocrystals under 365 nm excitation. Inset: aqueous solution of Ge nanocrystals excited at the same wavelength. c) Photoluminescence spectra under diverse excitation wavelengths, indicating excitation-dependent luminescence. d) Time-resolved PL spectra of Ge nanocrystals measured at different emission wavelengths. e) pH-dependent PL emission intensity at 395 and 445 nm. Insets are the solutions of Ge nanocrystals at various pHs.

446 nm originate from the two different crystalline forms of Ge nanocrystals; however, assigning the origin of these peaks to the contributing molecular species exactly is difficult. The photoluminescence quantum yield at 446 nm emission was calculated to be 26% and was determined by employing a quinine sulfate emission standard (Figure S4).[17] This result is significantly higher than the previously reported values of traditionally prepared Ge nanocrystals.[12a,c]

Previously cited factors that affect the luminescent properties of Ge nanocrystals include size,[11a,12a,13,16a,18] interfacial defects, surface oxides, matrix effects and the formation of ultra-small molecule-like Ge clusters (even though they are closely correlated with the formation of the crystals).[11b,19] Most reported Ge nanocrystals typically exhibit a size-dependent emission in the visible or NIR regions. However, no significant size effect has been observed for the Ge nanocrystals synthesized in our work. If PVP (Mw = 8 000) was used instead of PVP (Mw 58,000) in the synthesis, Ge nanocrystals with smaller size (1.5–4.5 nm) could be obtained with almost identical photoluminescence characteristics (Figure S5). Instead of size, we speculated that surface chemistry may play a major role in our case. Acidifying the Ge nanocrystal solution with HCl caused quenching of the photoluminescence emission peaks at both 445 and 395 nm, with the most dramatic change occurring between pH 5 and 6 (Figure 3e). Zeta potential measurements (Figure S6) indicated that the Ge nanocrystal surface changed from negatively charged to nearly neutral during the acidification, and this change may lead to photoluminescence quenching via non-irradiative recombination.[20] Moreover,

chemical modifications of the crystal surface may trap carriers or induce Ge/O related defects in the nonhomogeneous strain field of the crystal surfaces,[19f] so surface defects are expected to influence the emission. Crystalline form may be another important factor, as the two different observed emissions could correspond with the cubic and β-Sn tetragonal structures of Ge nanocrystals. Further investigation is needed to completely unveil the luminescence mechanism.

The optical behavior of the Ge nanocrystals was further examined by time-resolved photoluminescence spectroscopy to provide insight into the photo-generated charge recombination pathways of the materials (Figure 3d). Emission was monitored between 390 and 450 nm in 10 nm intervals. All photoluminescence decays required a three-component exponential fit, suggesting the existence of multiple de-excitation processes in the Ge nanocrystals. Time constants and relative amplitudes determined by the fit were summarized in Table S2. Contributions with time constants between 1 to 2 ns and 4 to 5 ns increased as the monitored emission wavelength increased. These effects became dominant before 450 nm, which is consistent with other reports.[12c] The origin of the multi-exponential optical behavior of the colloidal Ge nanocrystals is still unclear. According to Maria et al., the surrounding environment and surface composition of Ge nanocrystals could affect the efficiency of core electron-hole recombination and, consequently, fluorescence decays and dynamics.[21]

Photostability tests were performed by mounting the Ge nanocrystals in the focus of a 1000 W xenon lamp at full spectrum. Photoluminescence spectra of Ge nanocrystals taken during the phototreatment (Figure S7) indicated that the extremely intense illumination indeed induced instability in the Ge nanocrystals, especially for the emission peak at 446 nm with a loss in its initial photoluminescence intensity of more than 50% in one hour. Despite having a much lower quantum yield (4%) (Figure S4), the emission at 395 nm (with 320 nm wavelength excitation) was relatively more resistant to photobleaching. One possible cause is that ambient oxygen could penetrate through the polymer protective layer to the encapsulated nanocrystals. The photostability differences between the two emissions may be due to the different tendencies to oxidize. While, compared with the Ge nanocrystals, the fluorescence of reference dye sodium fluorescein was almost totally disappeared with one hour (Figure S7).

3. Cytotoxicity and Confocal Microscopy Images of Intracellular Acidic Compartments In Vitro

To assess the potential applications of the synthesized Ge nanocrystals in biological systems, cytotoxicity tests were performed to investigate their biocompatibility. Mitochondrial activity of A549 cells (a human lung cancer cell line) and B16 cells (a mouse melanoma cell line) was monitored after 24 h exposure to 0 to 200 μg/mL of Ge nanocrystals at 37 °C using a CCK-8 assay. The results showed that the Ge nanocrystals exhibited no observable cytotoxicity under the experimental condition (Figure S8). Longer incubation was also applied, and no measurable cytotoxicity was observed (data not shown). The biocompatibility of the Ge nanocrystals is promoted by our use of exclusively non-toxic reagents, especially using GeO_2 as the Ge precursor instead of the toxic organogermanium or germanium halide alternatives, as well as omission of any organic solvents that would be involved in phase transfers before application. On the contrary, alkylamine modified water-soluble Ge nanocrystals possessed high toxicity in cells, as reported by Ma et al.[22]

In addition to cell labeling and membrane protein tracking, intracellular imaging with the photoluminescent Ge nanocrystals has also received great attention. Some cell organelles and components, such as intracellular molecules, nuclear antigens, microtubules, actin filaments, have been labeled and monitored by photoluminescent nanocrystals.[2,3] To the best of our knowledge, most, if not all, lysosomal enzymes are acid hydrolases, and an inappropriate inner pH value will seriously affect the normal function of these lysosomes.[23] Because the Ge nanocrystals exhibited excellent pH-dependent fluorescence, particularly between pH values of 5 and 6, they may act as potential lysosomal pH sensors. Currently several lysosome-tracking dyes have been commercialized.[24] However, few attempts using Ge nanocrystals for lysosome sensing have been made (except for several reports related to cell pH sensors).[25] A series of cell imaging experiments were conducted to assess the Ge nanocrystals utility for this possible application. Cells were pretreated with different concentrations of bafilomycin A1, a specific inhibitor of vacuolar-type H(+)-ATPase, to inhibit the acidification of the lysosomes for 6 h before being loaded with the Ge nanocrystals.[26] The acidity of the lysosomes was also assessed with LysoSensor™ Green DND-189, an acidotropic probe that exhibits an increase in fluorescence intensity upon acidification. As shown in **Figure 4**, the LysoSensor fluorescence was only slightly dimmed in the cells pretreated with different concentrations of the inhibitor, demonstrating a relatively small elevation of lysosomal pH induced by bafilomycin A1. As comparison, the fluorescence of the Ge nanocrystals has been greatly enhanced in the cells pretreated with the various concentrations of bafilomycin A1. Notably, this enhancement appears to be dependent on the inhibitor concentration. These concentration dependent changes of fluorescence intensity suggest that the subtle pH alteration brought about by different concentrations of bafilomycin A1 can be better visualized with Ge nanocrystals than with LysoSensor. About a fourfold increase in fluorescence intensity was observed in Ge nanocrystals labeled cells, while the intensity of LysoSensor labeled cells decreased less than 50% in the B3 (cells were pretreated with Bafilomycin A1 at 5 μg/mL) treatment by semi-quantitative analysis. It should be noted that the two fluorescence signals (blue and green) demonstrated significant overlap, suggesting that the Ge nanocrystals were translocated via the lysosomal pathway after internalization. The merge images displayed a clear trend of the blue signal's increasingly outshining the green signal progressing from B1 to B3 treatments. This result is due to

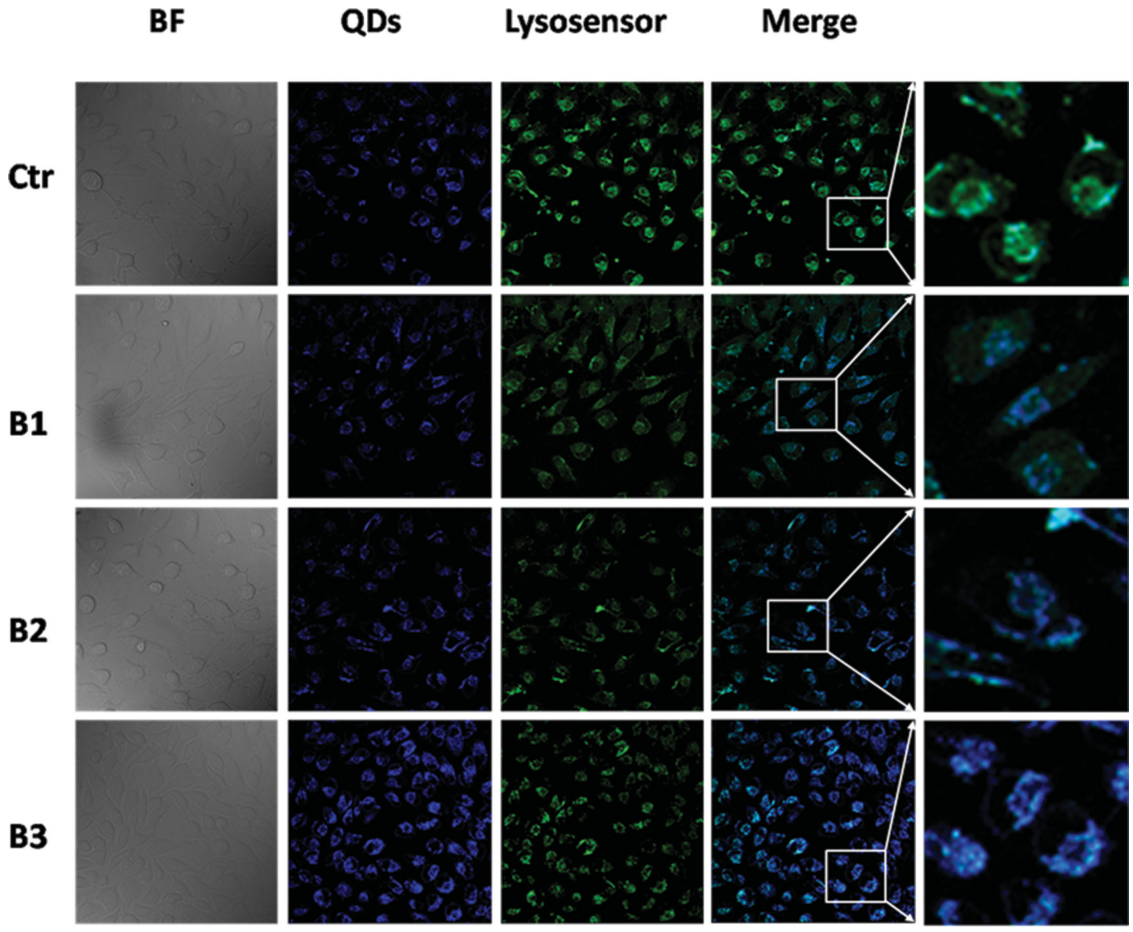

Figure 4. Confocal microscopy images of an intracellular acidic compartment of A549 cells. The cells were pretreated with Bafilomycin A1 at different concentrations (B1, B2, and B3 stand for 0.2, 1 and 5 μg/mL, respectively).

the blue fluorescence intensity's increasing and the green fluorescence intensity's decreasing[27] with a decline in the lysosomal acidity.

4. Conclusions

Blue-emitting pH-sensitive Ge nanocrystals were synthesized using facile aqueous solution based route without the use of a toxic Ge precursor, high temperature or expensive experimental conditions to protect from gases. From their luminescence profile and crystallographic properties, we suggested that the emission of the resulting Ge nanocrystals depends on both core- and surface-related properties. These photoluminescent Ge nanocrystals displayed a significantly enhanced photoluminescent quantum yield compared to those reported in previous literature and no observable toxicity at cell level. Further investigation explored the application of the pH-dependent fluorescence properties of these Ge nanocrystals to monitor the acidity of lysosomes in live cell images. The fluorescence of the Ge nanocrystals underwent great enhancement in the cell imaging experiments, even when the lysosomal pH was increased only slightly. These results demonstrated the potential of these Ge nanocrystals as an alternative lysosome pH sensor in biological fluorescence imaging. Moreover, in general, these nanocrystals' superior fluorescence properties and bioapplicability render them a promising bioimaging agent.

5. Experimental Section

Materials: All commercial materials were used as received. The bafilomycin A1 and all the reagents used in the synthesis of the Ge nanocrystals were purchased from Aldrich. LysoSensor Green DND-189 was purchased from Invitrogen Corporation.

Synthesis of Ge Nanocrystals: The Ge nanocrystals were prepared as follows. Firstly, 0.26 g GeO_2 was dissolved in 10 mL 0.6 mg/mL NaOH solution under ultrasonication to prepare aqueous Na_2GeO_3. The pH of the solution was adjusted to 6.5 with HCl. Then, 25 mg polyvinylpyrrolidone (PVP Mw = 58–000) was dissolved in 9 mL $NaBH_4$ solution while stirring, followed by injection of 1 mL of prepared Na_2GeO_3 solution. After adding Na_2GeO_3, the colorless aqueous solution turned to yellow-green, which further changed to red-orange. Afterwards, a large amount of brown-red precipitate formed. The pH of the mixture was adjusted to the range of 8–9 to dissolve the precipitate and was incubated in an oil bath at 80 °C for 8 h, finally generating the colorless Ge nanocrystals.

Ge Nanocrystals Characterization: Absorption and fluorescence spectra were recorded on a Lambda 950 UV/Vis spectrophotometer (Perkin–Elmer) and a LS 55 fluorescence spectrometer. The

morphology was obtained by depositing the sample on a carbon-coated copper grid, and then examining with a transmission electron microscope (TEM, Tecnai G2 20 S-TWIN, FEI, USA). Fourier transform infrared spectra were recorded on Perkin-Elmer Spectrum One FTIR Spectrometer after the sample was freeze-dried. The size was determined using a ZetaSizer Nano series Nano-ZS (Malvern Instruments Ltd., Malvern, UK) with a measure range from 0.6 nm to 6 μm. Time-resolved decays were measured using a Nanolog-TCSPC (Horbia JY, Japan) spectrofluoremeter, and an excitation wavelength at 377 nm was used in all cases. Ge 3d photoemission spectra were recorded on ESCALAB250Xi X-ray surface photoelectron spectroscopy (XPS) after the sample was freeze-dried. XRD patterns were obtained for 10–90° by continuous-scanning with a step size of 0.02° and speed of 2° min^{-1} on D/max-TTRIII with Cu-Kα radiation (Rigaku, Japan) at a scanning step size of 0.05°/2θ.

Quantum Yield Calculation: Integrated PL intensities versus absorbance for multiple diluted Ge nanocrystals in ultra-pure water and for various dilutions of quinine sulfate in 0.05 M H_2SO_4 under identical excitation wavelength (365 nm) are shown in Figure S4. The quantum yield was calculated from the ratio of the slopes of the linear fits of the Ge nanocrystal and quinine sulfate data and the known quantum yield of quinine sulfate (54.6%) at 365 nm.

Cell Culture: The human lung cancer cell line A549 cells and mouse melanoma cell line B16 cells were maintained at 37 °C (5% CO2) in Dulbecco's Modified Eagle's Medium (DMEM, HyClone) supplemented with 10% (vol/vol) fetal bovine serum (Gibco), 2 mM L-glutamine, 20 mM HEPES, 100 U/mL penicillin and 1 mg/mL streptomycin.

Cell Viability: The cells were seeded in 96-well plates at 37 °C. A cell count kit-8 (CCK-8) (Kumamoto Techno, Japan) was used to examine cell viability. CCK-8 includes WST-8 [2-(2-methoxyl-4-nitrophenyl)-3-(4-nitrophenyl)-5 -(2,4-disulfonicacid benzene)-2H-tetrazolium sodium] which can be reduced to a highly water-soluble formazan dye by living cells. The amount of dye formed is directly proportional to the number of living cells. After treatment 24 h or longer, the medium was removed and 100 μL DMEM containing CCK-8 (10%, vol/vol) was added to each well. After 1 h incubation at 37 °C, the absorbance at 450 nm of each well was measured using a microtiter plate reader (TECAN Infinite M200, Austria).

Confocal Microscopy: Cells were seeded onto coverslips at the bottom of tissue culture dishes and pretreated with as needed. Ge nanocrystals were loaded at the concentration of 50 μg/mL after the cells were incubated with Bafilomycin A1 at different concentrations (0.2, 1 and 5 μg/mL, respectively) for 4 h at 37 °C. Afterward, the cells were further co-incubated with nanocrystals and Bafilomycin A1 at 37 °C for 10 h, the media were removed and replaced with fresh media containing LysoSensor™ Green DND-189 (1 μg/mL). After 30-min incubation, the loading solution was replaced with fresh media and the cells were observed using a Nikon Ti-e microscope with an UltraVIEW Vox (PerkinElmer) confocal attachment using a 601.4 NA Plan Apochromat oil immersion lens.

Supporting Information

Supporting Information is available from the Wiley Online Library or from the author.

Acknowledgements

This work was supported by the grants from National Basic Research Plan of China (MoST 973 Program 2012CB934004, 2010CB933601), the National Natural Science Foundation of China (31325010 and 21273126) and Open Research Fund Program of the State Key Laboratory of Low-Dimensional Quantum Physics (KF201311). The authors thank Prof Xiaohui Qiu and Yingying Xu, from NCNST, for their help for time-resolved photoluminescence spectroscopy measurement.

[1] a) M. Bruchez, M. Moronne, P. Gin, S. Weiss, A. P. Alivisatos, *Science* **1998**, *281*, 2013; b) W. C. W. Chan, Nie, S. M. *Science* **1998**, *281*, 2016.

[2] a) I. L. Medintz, A. R. Clapp, H. Mattoussi, E. R. Goldman, B. Fisher, J. M. Mauro, *Nat. Mater.* **2003**, *2*, 630; b) A. P. Alivisatos, *Nat. Biotechnol.* **2004**, *22*, 47; c) K. E. Sapsford, T. Pons, I. L. Medintz, H. Mattoussi, **2006**, *6*, 925; d) R. J. Martín-Palma, M. Manso, V. Torres-Costa, **2009**, *9*, 5149.

[3] a) Y. C. Wang, R. Hu, G. M. Lin, I. Roy, K. Yong, *ACS Appl. Mater. Interfaces* **2013**, *5*, 2786; b) Z. Yue, F. Lisdat, W. J. Parak, S. G. Hickey, L. P. Tu, N. Sabir, D. Dorfs, N. C. Bigall, *ACS Appl. Mater. Interfaces* **2013**, *5*, 2800; c) X. G. Peng, J. Thessing, *Struct. Bonding* **2005**, *118*, 79.

[4] a) S. W. Kim, J. P. Zimmer, S. Ohnishi, J. B. Tracy, V. Frangioni, M. G. Bawendi, *J. Am. Chem. Soc.* **2005**, *127*, 10526; b) J. Wang, S. Q. Sun, F. Peng, L. X. Cao, L. F. Sun, *Chem. Commun.* **2011**, *47*, 4941; c) N. Pradhan, D. M. Battaglia, Y. C. Liu, X. G. Peng, *Nano Lett.* **2007**, *7*, 312; d) M. Geszke, M. Murias, L. Balan, G. Medjandi, J. Korczynski, M. Moritz, J. Lulek, R. Schneider, *Acta Biomater.* **2011**, *7*, 1327; e) J. H. Park, L. Gu, G. Von Maltzahn, E. Ruoslahti, S. N. Bhatia, M. J. Sailor, *Nat. Mater.* **2009**, *8*, 331; f) K. T. Yong, H. Ding, I. Roy, W. C. Law, E. J. Bergey, A. Maitra, P. N. Prasad, *ACS Nano* **2009**, *3*, 502.

[5] a) J. Wang, Y. X. Liu, F. Peng, C. Y. Chen, Y. H. He, H. Ma, L. X. Cao, S. Q. Sun, *Small* **2012**, *8*, 2430; b) L. Brus, *Adv. Mater.* **1993**, *5*, 286; c) M. J. Sailor, K. L. Kavanagh, *Adv. Mater.* **1992**, *4*, 432; d) L. talmans, J. Poortmans, H. Bender, M. Caymax, K. Said, E. Vazsonyi, J. Nijs, R. Mertens, *Prog. Photovolt. Res. Appl.* **1998**, *6*, 233; e) M. J. Sailor, E. J. Lee, *Adv. Mater.* **1997**, *10*, 783; f) H. Okamoto, Y. Sugiyama, H. Nakano, *Chem. Eur. J.* **2011**, *17*, 9864; g) J. Heitmann, F. Müller, M. Zacharias, *Adv. Mater.* **2005**, *7*, 803; h) Z. Y. Brus, R. Friesner, *Nano Lett.* **2003**, *3*, 163; i) M. Rosso-Vasic, E. Spruijt, B. Lagen, L. D. Cola, H. Zuilhof, *Small* **2008**, *4*, 1835; j) E. J. Henderson, A. J. Shuhendler, P. Prasad, V. Baumann, F. Maier-Flaig, D. O. Faulkner, U. Lemmer, X. Y. Wu, G. A. Ozin, *Small* **2011**, *7*, 2507.

[6] a) J. P. Wilcoxon, P. P. Provencio, G. A. Samara, *Phys. Rev. B.* **2001**, *64*, 035417; b) J. P. Wilcoxon, P. P. Provencio, G. A. Samara, *Phys. Rev. B.* **1999**, *60*, 2704; c) J. H. Wu, Y. G. Sun, R. J Zou, G. S. Song, Z. G Chen, C. R Wang, J. Q Hu, *CrystEngComm* **2011**, *13*, 3674.

[7] Y. Maeda, N. Tsukamoto, Y. Yazawa, Y. Kanemitsu, Y. Masumoto, *Appl. Phys. Lett.* **1991**, *59*, 3168.

[8] a) E. J. Henderson, C. M. Hessel, J. G. C. Veinot, *J. Am. Chem. Soc.* **2008**, *130*, 3624; b) E. J. Henderson, C. M. Hessel, R. G. Cavell, J. G. C. Veinot, *Chem. Mater.* **2010**, *22*, 2653.

[9] X. Lu, K. J. Ziegler, A. Ghezelbash, K. P. Johnston, B. Korgel, *Nano Lett.* **2004**, *4*, 969.

[10] E. Fok, M. Shih, A. Meldrum, J. G. C. Veinot, *Chem. Commun.* **2004**, *10*, 386.

[11] a) B. R. Taylor, S. M. Kauzlarich, G. R. Delgado, H. W. H. Lee, *Chem. Mater.* **1999**, *11*, 2493; b) B. R. Taylor, G. A. Fox, L. J. Hope-Weeks, R. S. Maxwell, S. M. Kauzlarich, H. W. H. Lee, *Mater. Sci. Eng. B* **2002**, *96*, 90.

[12] a) D. C. Lee, Pietryga, J. M. I. Robel, D. J. Werder, R. D. Schaller, V. I. Klimov, *J. Am. Chem. Soc.* **2009**, *131*, 3436; b) E. J. Henderson, M. Seino, D. P. Puzzo, G. A. Ozin, *ACS Nano* **2010**, *12*, 7683; c) J. H. Warner, R. D. Tilley, *Nanotechnology* **2006**, *17*, 3745; d) N. H. Chou, K. D. Oyler, N. E. Motl, R. E. Schaak, *Chem. Mater.* **2009**, *21*, 4105.
[13] H. Gerung, S. D. Bunge, T. J. Boyle, C. J. Brinker, S. M. Han, *Chem. Commun.* **2005**, 1914.
[14] a) M. Baublitz, A. L. Ruoff, *J. Appl. Phys.* **1982**, *8*, 5669; b) Y. Saito, *J. Cryst. Growth* **1979**, *47*, 61.
[15] a) J. S. Kasper, S. M. Richards, *Acta Cryst.* **1964**. *17*, 752; b) Caculated from ICSD using POED-12++[1997].
[16] a) J. P. Wilcoxon, P. P. Provencio, G. A. Samara, *Phys. Rev. B.* **2001**, *64*, 0354171; b) J. R. Heath, J. J. Shiang, A. P. Alivisatos, *J. Chem. Phys.* **1994**, *101*, 1607.
[17] a) R. M. Sankaran, D. Holunga, R. C. Flagan, K. P. Giapis, *Nano Lett.* **2005**, *5*, 537; b) J. N. Demasa, G. A. Crosby, *J. Phys. Chem. C.* **1971**, *8*, 991.
[18] E. B. Gorokhov, V. A. Volodin, D. V. Marin, D. A. Orekhov, A. G. Cherkov, A. K. Gutakovskii, V. A. Shvets, A. G. Borisov, M. D. Efremov, *Semiconductors* **2005**, *39*, 1168.
[19] a) H. P. Wu, M. Y. Ge, C. W. Yao, Y. W. Wang, Y. W. Zeng, L. N. Wang, G. Q. Zhang, J. Z. Jiang, *Nanotechnology* **2006**, *17*, 5339; b) M. Zacharias, P. M. Fauchet, *Appl. Phys. Lett.* **1997**, *71*, 380; c) K. Yoshihiko, U. Hiroshi, M. Yasuaki, M. Yoshihito, *Appl. Phys. Lett.* **1992**, *61*, 2187; d) H. Yang, R. Yang, X. Wan, W. Wan, *J. Cryst. Growth* **2004**, *261*, 549; e) A. G. Cullis, L. T. Canham, P. D. J. Calcott, *J. Appl. Phys.* **1997**, *82*, 909; f) M. Zacharias, P. M. Fauchet, *J. Non-Cryst. Solids* **1998**, *227*, 1058.
[20] C. Galland, Y. Ghosh, A. Steinbrück, M. Sykora, J. A. Hollingsworth, V. I. Klimov, H. Htoon, *Nature.* **2011**, *479*, 203.
[21] M. J. Ruedas-Rama, A. Orte, E. A. H. Hall, J. M. Alvarez-Pez, E. M. Talavera, *ChemPhysChem* **2011**, *12*, 919.
[22] Y. H. Ma, C. P. Huang, J. S. Tsai, M. Y. Shen, Y. K. Li, L. Y. Lin, *Toxicol. Lett.* **2011**, *207*, 258.
[23] G. M. Cooper, The Cell: A Molecular Approach. 2nd ed, Sinauer Associates, Sunderland, MA **2000**; Lysosomes. Available from http://www.ncbi.nlm.nih.gov/books/NBK9953/ (accessed: September **2006**).
[24] R. Sabnis, *Handbook of Acid-Base Indicators*, CRC Press, Boca Raton **2007**, pp 416.
[25] a) A. Orte, J. M. Alvarez-Pez, M. J. Ruedas-Rama, *ACS Nano* **2013**, *7*, 6387; b) M. F. Gui, L. J. Bao, Y. S. Xia, C. Wei, S. Z. Zhang, C. Q. Zhu, *Biosen. Bioelectron.* **2011**, *30*, 324.
[26] T. T. Yoshimori, A. A. Yamamoto, Y. Y. Moriyama, M. M. Futai, Y. Y. Tashiro, *J. Biol. Chem.* **1990**, *265*, 21940.
[27] E. Gulbins, Y. Zhang, X. Li, H. Grassmé, G. Döring, E. Gulbins, *J. Immunol.* **2010**, *184*, 5104–5111.

Received: September 11, 2014
Revised: October 11, 2014
Published online: January 12, 2015

